Title

Frequency and damping effect of suspended silicon nitride membranes in water near the megahertz range

Journal

Journal of Micromechanics and Microengineering, 30(12)

ISSN

0960-1317

Authors

Wang, Jiaying
Mei, Jiyang
Friend, James
et al.

Publication Date

2020-12-01

DOI

10.1088/1361-6439/abbcba

Peer reviewed

Frequency and damping effect of suspended silicon nitride membranes in water near the megahertz range

Jiaying Wang,[1,2,3] Jiyang Mei,[4,5] James Friend,[4,5,6,a)] and Oscar Vazquez-Mena[1,2,3,b)]
[1)] *Department of Nanoengineering, University of California, San Diego, La Jolla, CA 92093, United States*
[2)] *Center for Memory and Recording Research, University of California, San Diego, La Jolla, CA 92093, United States*
[3)] *Calibaja Center for Resilient Materials and Systems, University of California, San Diego, La Jolla, CA 92093, United States*
[4)] *Department of Mechanical Aerospace and Engineering, University of California, San Diego, 9500 Gilman Drive, La Jolla, CA 92093, United States*
[5)] *Materials Science and Engineering, University of California, San Diego, La Jolla, CA 92093, United States*
[6)] *Medically Advanced Devices Laboratory, Center for Medical Devices and Department of Surgery, School of Medicine, University of California, San Diego, La Jolla, CA 92093, United States*

(Dated: 20 January 2022)

Understanding the behavior of water-immersed membranes in the megahertz range is critical to develop novel acoustic metamaterials compatible with biomedical ultrasound applications. Herein, we study the influence of water on the resonance frequency and quality factor near the megahertz range of silicon nitride membranes fully immersed in water using Laser Doppler Vibrometry. The resonance frequency of silicon nitride membranes significantly decreases in water compared to air. For a 40 μm wide membrane, the resonance frequency is reduced from 11.2 MHz in air to 1.24 MHz after immersion in water, which is confirmed by finite element method simulations. Our results indicate that the water mass loading plays a major role in the resonance frequency reduction, with a ratio of water mass to membrane mass of $m_{\text{water}}/m_{\text{membrane}} \sim 10^2$ and NAVMI factors of $\Gamma \sim 1.3$. We attribute the main losses to acoustic radiation with small contributions from viscous damping. We estimate that silicon nitride membranes with widths below 50 μm are required to build negative metamaterials operating above 1 MHz. The large NAVMI factors suggest strong coupling between membrane motion and acoustic waves in water, which is important to develop metamaterials able to manipulate acoustic fields.

I. INTRODUCTION

Membranes have emerged as crucial components to obtain effective negative density in acoustic metamaterials by inducing opposite phase between pressure and acceleration.[1–4] Hyperbolic metamaterials with negative effective density built by two-dimensional membrane arrays have enabled super lenses with resolution beyond the diffraction limit at 1 kHz.[5] When membranes enabling negative density are combined with Helmholtz resonators producing negative effective modulus[6], double negative metamaterials (i.e. negative density and negative modulus) can be obtained.[7,8] These extraordinary materials are predicted to enhance acoustic transmission through high-contrast biological barriers such as the skull,[9] which could enable novel capabilities in biomedical ultrasound such as non-invasive neurostimulation and transcranial brain imaging and therapies. However, the experimental realization of negative acoustic metamaterials has not reached the operating frequency of medical ultrasound. The implementation of membranes with resonance frequency in the MHz range in water is one of the major challenges which needs to be solved.

Silicon nitride (SiN_x) membranes are widely used as mechanical resonators in microelectromechanical systems (MEMS) and have broad applications such as pressure sensors and transducers, membrane sieves, microresonators, and microfabrication shadow masks[10–17]. They are remarkably strong against static loads and chemically stable in a wide range of environments.[18] These properties make SiN_x a natural candidate to produce membrane components in acoustic metamaterials operating in high-frequency range. There are several studies on SiN_x membranes used as capacitive ultrasound transducer[19,20], filters[16], and pressure sensors[21], but there are no specific studies on their resonance behavior in the MHz range fully immersed in water. Solid plates dominated by flexural rigidity immersed in liquid have also been studied[22], but the resonance frequency of membranes with residual tensile stress operating fully immersed in water still near the MHz range remains largely unexplored. The main limitation to achieve MHz resonance frequency is the strong reduction in resonance frequency of mechanical resonators upon immersion.[23–25] The main factors causing this reduction are the kinetic energy transfer from the membrane to the liquid and the viscous losses.[26,27] Understanding the resonance frequency reduction of SiN_x

[a)] Electronic mail: jfriend@eng.ucsd.edu
[b)] Electronic mail: oscarvm@eng.ucsd.edu

membranes and damping phenomena are important for their implementation in acoustic metamaterials for ultrasound imaging applications.

Herein, we study the reduction in resonance frequency and quality factor of SiN_x membranes from air to water. Previous reports have suggested that unit cells in the 100 μm range could operate around 1 MHz in water[5], therefore, we decided to study membranes with widths around 100 μm, fabricating membranes with widths between 40 and 160 μm wide. The membrane vibrations are studied using Laser Doppler Vibrometry (LDV), allowing measuring the resonance frequency and imaging their respective vibration modes. We also use finite element methods (FEM) to simulate the behavior of the membranes. From the experimental values of resonance frequency and quality factor (Q factor) we extract the water loading added mass, the non-dimensionalzed added virtual mass incremental (NAVMI) factor, the damping ratio and the damping coefficient for different vibrating modes of membranes with different sizes. The estimated NAVMI factor and damping coefficients are crucial parameters that will facilitate the design of SiN_x membranes for negative acoustic metamaterials close to relevant medical ultrasound frequencies.

II. METHODS

The membranes were designed with square shape and widths of 40, 80, 120 and 160 μm aiming to reach resonance frequencies around 1 MHz in water. Fig. 1(a) illustrates the microfabrication of the suspended SiN_x membranes for this study which is based on conventional KOH etching. Our process starts with a 400 μm-thick, double-sided polished silicon wafer (4-inch (100) silicon wafer, University Wafer Inc., MA, US) with 200 nm-thick SiN_x layers deposited on both sides by low-pressure chemical vapor deposition. Then, a chrome metallic layer is deposited on the top (membrane) side to protect the top SiN_x during wafer processing. Ultraviolet photolithography was then carried out on the back side of the wafer with a positive photoresist (AZ12XT-10PL, Microchemicals, Ulm, Germany), followed by SiN_x dry etching on the backside to define opening windows for KOH etching. Then the photoresist and Cr protective layer are removed. Finally, the topside SiN_x thin film was released by KOH wet anisotropic Si etching (40 wt%, 80 °C, 5 hrs). The wafer is cleaned in a HCl bath for 30 min for potassium decontamination followed by RCA cleaning. Fig. 1(b1)-(b4) shows an optical microscope image of four membranes with different membrane widths on the front side of the chip. Due to fabrication process limitations, the final membranes had slight variations from the designed values. For example, the membranes in Fig. 1(b1)-(b4) have actual sizes of 39 μm, 82 μm, 118 μm and 157 μm in width. An important aspect from the fabrication are variations in thickness. Supplementary information (Fig. SI-1) shows the experimental mapping and thickness fitting data from ellipsometry (J.A. Woollam M-2000D Ellipsometer) confirming the thickness of 204 nm with a variation of ± 2 nm. Fig. SI-2 also shows that the thickness of the SiN_x layer is 200 nm. It also shows SEM images of the 39 μm wide suspended membrane morphology from the backside of the silicon substrate, showing the KOH cavities.

LDV measurements[28–30] were performed with a UHF-120SV equipment (Polytec, Waldbronn, Germany) with the measurement setup shown in Fig. 1(c). The membranes were excited by a 4 by 4 cm square shape lithium niobate thickness-mode device with an adhesive putty absorber between the lithium niobate and the silicon chip hosting the membrane. The distance between the lithium niobate and the membrane was set at 1 cm to prevent dynamic or near-field coupling between the membrane and transducer, ensuring that any vibration in the membrane is induced via the fluid.[31] The excitation from the water on the Si frame is expected to be negligible in comparison to the water-membrane coupling given the large acoustic impedance difference between water and silicon. The membranes were excited with a chirp wave by a vector signal generator (SMBV100A, Rohde Schwarz, Germany) and an amplifier (ZHL–32A+, Mini-Circuits, Brooklyn, NY) before being applied to the face electrodes of the lithium niobate. Frequency sweeps were performed from 9 kHz to 20 MHz in air and from 9 kHz to 4 MHz in water with 625 Hz steps in both cases. The chirp wave period was set to 1.6 ms to match the average time elapsed between each LDV measurement from point to point as it scanned across the membrane. Each displacement measurement was averaged ten times to reduce the potential signal noise. Four samples for each membrane dimension were measured from which the average and standard deviation of the resonance frequency and Q factor were extracted. Size variations were mainly due to the fabrication process. Lorentzian distributions curve fitting characteristic of resonance responses of dynamic systems were utilized to extract the peak position and Q factor for each resonance. The experimental Q factor is calculated by $Q_{\text{exp}} = f_{\text{R}}/(f_2 - f_1)$ where f_1 and f_2 are frequencies at which the amplitude of is $1/\sqrt{2}$ times of the resonance frequency f_{R}. Since our LDV setup produces a laser spot of 3 μm in diameter, we were able to study the (1,1), (1,2), (1,3)+(3,1), (1,4) of the membranes. However, in the particular case of the 39 μm wide membranes, the laser spot was too wide to resolve the (1,3)+(3,1) and (1,4) modes.

Simulations in air were performed using the built-in thermo-acoustics model in COMSOL Multphysics, considering the thermal and viscous damping effect in water. The linearized Navier-Stokes equation was solved with the thermoviscous boundary layer condition. The thickness of the thermo-viscous boundary layer is set as $\delta_v = 0.57(\mu\text{m})\frac{1(\text{MHz})}{f}$ where f is working frequency[32]. The velocity of sound in water is 1480 m/s and bulk viscosity is 2.47×10^{-3} Pa·s.[33] The resonance frequency and quality factor can be obtained by eigenfrequency simula-

tion. For each multimode vibration shape, the resonance frequency is calculated by FEM resulting in a complex number frequency ($f_R = f_{real} + if_{imag}$). The real part ($f_{real}$) represents the resonance frequency and the imaginary part (f_{imag}) shows the dissipation. Thus, the Q factor at resonance can be obtained from $Q = f_{real}/(2f_{imag})$.

III. RESULTS AND DISCUSSION

The LDV characterizaton of an 82 μm wide SiN_x membrane is shown in Fig. 2, showing the resonance frequency and Q factor in air and water. Fig. 2(a-c) show the normalized displacements and mode shapes of the membrane in air with Lorentzian fittings for the resonance peaks. The resonance frequencies in air for (1,1), (1,2) and (1,3)+(3,1) modes are $f_{1,1}^{air} = 5.38$ MHz, $f_{1,2}^{air} = 8.49$ MHz and $f_{1,3}^{air} = 12.3$ MHz. The mode (1,3)+(3,1) is actually a superposition of the natural (1,3) and (3,1) modes as discussed in the Supplementary Information in Fig. SI-3. In the case of the (1,2) modes, there might be also some superposition of the (1,2) and (2,1) modes, also discussed in the Supplementary Information in Fig. SI-4. Fig. 2(d-f) show the results for the same membrane, 82 μm wide, immersed in water. The drastic decrease in resonance frequency from air to water is evident. The (1,1) mode frequency is reduced by ∼10x from $f_{1,1}^{air} = 5.38$ in air to $f_{1,1}^{water} = 0.44$ MHz in water. Similarly, the resonance frequency for the higher modes are reduced from 8.49 to 1.17 MHz for the (1,2) mode, and from 12.3 to 1.87 MHz for the (1,3)+(3,1) mode. The Q factor is also reduced after water immersion. For the (1,1) mode, Q reduces from 138.1 to 5.31, illustrating the strong damping forces affecting the motion of the membrane in water.

We compared experimental LDV measurements with analytical calculations and FEM simulations. Fig. 3(a) shows the resonance frequency as function of membrane width for the (1,1) mode, exhibiting good agreement between experimental measurements in air by LDV (red squares), FEM simulation in air (red line), and analytic theoretical values (black dotted line). The theoretic resonance frequency values of membranes are extracted by the following equation:[34]

$$f_{i,j}^{air} = \{\frac{\lambda_{i,j}^4}{4\pi^2 a^4}\left[\frac{Eh^2}{12\rho(1-\nu^2)}\right] + \frac{N(J_i+J_j)}{4\rho h a^2}\}^{1/2} \quad (1)$$

where a is the membrane width, and $h = 200$ nm is the thickness; $\rho = 3170$ kg/m^3 and $\nu = 0.23$ are the density and Poisson's ratio of silicon nitride; $f_{i,j}^{air}$ is the natural frequency for i,j mode where i and j refer to the numbers of half-wavelengths present in the mode shape along the x and y axes; N is the linear tensile load; J_i is a constant that depends on the mode number and boundary condition (J_1 =1.248 for clamped membranes); $\lambda_{i,j}$ are geometrical parameters for the i and j modes.[34] The experimental and theoretical values for higher resonance modes are shown in the Figure SI-5 and listed in Table SI-1 in the Supplementary Information. The resonance values at different mode shapes show also a good agreement between experiments, simulations, and analytical result. The overall frequency mismatch between experimental and simulation results is less than 5%. A critical parameter that determines the membrane vibration behavior is its tensile stress. This value is calibrated by matching the calculations for resonance frequency from Eq. 1 with LDV measurements for various resonance modes. The calibrated value obtained from the (1,1) mode is 1.2 GPa. The results from higher modes (1,2) and (1,3)+(3,1) also confirm the stress of membrane of 1.2 GPa.

Fig. 3(a) clearly shows the drastic reduction of resonance frequency in water. For the (1,1) mode and for widths from 160 to 40 μm, the membranes in air (red line/squares) reach a frequency range of $\sim 2.59 - 11.2$ MHz, but after immersion in water, the range decreases to $\sim 0.18 - 1.24$ MHz (blue line/squares). Fig. 3(b) shows the ratio of frequencies in air to water ($f_{1,1}^{air}/f_{1,1}^{water}$) as function of width for the (1,1) mode. For 40 μm, the ratio $f_{1,1}^{air}/f_{1,1}^{water}$ is ∼9, while for 160 μm it reaches ∼14. This reduction in resonance frequency after water immersion is observed for higher resonance modes. Fig. 3(c) shows $f_{i,j}^{air}$ and $f_{i,j}^{water}$ for the higher resonance modes for a 118 μm wide membrane and Fig. 3(d) shows the corresponding $f_{i,j}^{air}/f_{i,j}^{water}$ ratios. The natural mode (1,1) shows the largest reduction with $f_{1,1}^{air}/f_{1,1}^{water}$ ∼15, while the higher (1,4) mode shows a smaller reduction with $f_{1,4}^{air}/f_{1,4}^{water}$ ∼6. The Q factor also shows a strong reduction for different widths and modes. For the (1,1) mode, the Q factor drops to $Q_{water} < 10$ for the all the membranes from 40 to 160 μm as shown in Fig. 3(e). In particular, the largest drop occurs for the smallest 40 μm membrane , dropping from $Q_{air} = 694$ to $Q_{water} = 5.6$. The Q factor for different modes of the 120 μm membranes is shown in Fig. 3(f). In addition, we explored the behavior of circular membranes by simulations since fabrication of circular membranes at this size scale poses more challenges. In the Supplementary Information in Fig. SI-6, we present the resonance frequencies for circular frequencies, $f_{1,1}^{air}$ and $f_{1,1}^{water}$, as well as the ratio of the frequencies ($f_{1,1}^{air}/f_{1,1}^{water}$) for diameters of 40, 80, 120 and 160 um. The results show the similar trends, with a drastic reduction in frequency from air to water. For 40 μm, the ratio $f_{1,1}^{air}/f_{1,1}^{water}$ is ∼7, while for 160 μm it reaches ∼15.

To analyze the reduction in frequency, we first look at the contribution from water loading that causes a transfer of kinetic energy from the membrane to the liquid. From the resonance frequency in water and mass, the added mass for mechanical resonators in liquid can be estimated from the expressions:[35]

$$\frac{f_{water}}{f_{air}} = \sqrt{\frac{m_{membrane}}{m_{membrane} + m_{water}}} \quad (2)$$

$$\frac{m_{\text{water}}}{m_{\text{membrane}}} = (\frac{f_{\text{air}}}{f_{\text{water}}})^2 - 1 \quad (3)$$

The ratio of the water added mass (m_{water}) over the membrane mass (m_{membrane}) as function of membrane width for different modes is plotted in Fig. 4(a). It increases as the width (a) increases, starting at $m_{\text{water}}/m_{\text{membrane}} = 80$ for a = 40 μm up to $m_{\text{water}}/m_{\text{membrane}} = 212$ for a = 120 μm, followed by slight decrease to 206 for a = 160 μm. The large ratios of $m_{\text{water}}/m_{\text{membrane}}$ indicate that the restoring elastic force of the membrane is also transferred to a water body much larger in mass than the membrane itself. For the higher (1,2) and (1,3)+(3,1) modes, the $m_{\text{water}}/m_{\text{membrane}}$ ratio decreases to a range from 25 to 100, with a closely linear increment as function of membrane width. The added mass can be quantified by the nondimensionalized added virtual mass incremental, or NAVMI, factor reflecting the ratio of kinetic energy of the water to the kinetic energy of the solid membrane[23]. The shift in resonance frequency and the NAVMI factor (Γ) are related by:[23]

$$\frac{f_{i,j}^{\text{water}}}{f_{i,j}^{\text{air}}} = 1/\sqrt{1 + \Gamma_{i,j}\beta} \quad (4)$$

$$\Gamma_{i,j} = \left[\left(\frac{f_{i,j}^{\text{air}}}{f_{i,j}^{\text{water}}} \right)^2 - 1 \right] \frac{1}{\beta}, \quad (5)$$

where $\beta = d\rho_w a/\rho h$ is a thickness correction factor and ρ_w is the water density. The NAVMI factor can be understood as a ratio between the membrane width a and the thickness of the water layer following the membrane motion l_w. The NAVMI factor is plotted in Fig. 4(b) as function of membrane width for different modes. As expected from the added mass values in Figure 4(a), the NAVMI values for the (1,1) mode are higher than for (1,2) and (1,3)+(3,1) modes. For the (1,1) mode, based on the NAVMI factor range of $\Gamma \sim 1.3 - 0.8$, it can be estimated that the water layer following the membrane motion is close to the actual width of the membrane. However, it should be stressed that the membrane is not in a symmetric environment. One side of the membrane faces the Si chip cavity with size ∼a, while the other side has an infinite opened geometry, therefore, the layers of water following the membrane can be different on the two sides. As the membrane is reduced, the Si cavity is also reduced and this may affect the NAVMI factor of smaller membranes. In the case of the higher (1,2) and (1,3)+(3,1) modes, the NAVMI factor is smaller and shows a behavior independent of size. For a given membrane width, the NAVMI factor clearly decreases for higher resonance modes as shown in Fig. 4(b). This is expected as the propagation in water of acoustic waves following higher membrane modes is more difficult compared with (1,1) mode that can easily couple to pressure acoustic waves. Previous reports on clamped circular plates (motion driven by flexural rigidity) in infinite open geometries have reported NAVMI values of $\Gamma = 0.35$ for natural (1,1) mode and lower values of $\Gamma < 0.3$ for higher order modes.[22] In our case, our natural (1,1) mode for squared clamped membranes gives a higher NAVMI factor, indicating a stronger coupling with water motion. The higher values in our case can be due to the cavity geometry on one side of the membranes, which may extend the water motion coupled to the membrane as compared with an infinite open geometry. Another reason for the larger NAVMI factor maybe that for our thin membranes, the restoring force is driven by residual stress that is thickness independent, whereas plates are driven by flexural rigidity that require thicker dimensions to achieve same restoring forces. Therefore, the ratio of water mass to membrane mass is expected to be higher than for plates.

The main damping mechanisms in water are acoustic radiation and viscous losses. The Reynolds number for our membranes can be expressed as:[36]

$$R_e = \frac{\rho_f \omega_{\text{water}} a^2}{4\mu}. \quad (6)$$

where ρ_f is the fluid density, ω_{water} is the angular frequency in water, and μ is the bulk viscosity. For the (1,1) mode ($\omega_{\text{water}} \sim 2\pi \times 10^6$ rad/s), we obtain $R_e = 3327$ for the 39 μm membrane and $R_e = 7826$ for the 157 μm membrane. These large Reynolds numbers suggest an low viscous fluid regime in which the main damping factor is the energy lost through acoustic radiation, which as mentioned earlier, seems probable due to the large NAVMI factor and added mass values. The damping ratio $\zeta = 1/(2Q)$ is shown in Fig. 4(c) as function of membrane width for different resonance modes. The damping ratio ζ is the highest for the (1,1) mode, reaching $\zeta \sim 0.1$. The (1,2) and (1,3)+(3,1) modes have smaller damping ratios of $\zeta = 0.01 - 0.03$. The damping behavior of these modes requires further studies since their motion is influenced by the super-position of the (1,2) and (2,1), and (1,3) and (3,1) modes, respectively. Understanding the contribution of each natural mode to the superposition is required to understand the damping of the membranes at their particular modes. The supplementary information (Fig. SI-3 and SI-4) contains images of these modes and the superposition result. Since $\zeta < 1$ for all cases, we can assume that the membrane oscillations are underdamped, which is crucial for the operation of the membranes as acoustic metamaterial components. The damping coefficients

$$\gamma = \frac{m_{\text{membrane}} + m_{\text{water}}}{Q} \omega_{\text{water}} \quad (7)$$

are shown in Fig. 4(d), showing a decrease as membrane width decreases. This is encouraging for acoustic metamaterials targeting operation above 1 MHz. Based on Fig. 4(d), it is possible that membranes below 40 μm can

reach higher frequencies without suffering strong overdamping, allowing effective interactions between membranes and acoustic waves.

IV. CONCLUSIONS

This work reports the significant reduction in resonance frequency when membranes with widths a=40−160 μm are immersed in water, reaching a ∼10x reduction factor. Based on our measurements, to achieve resonance frequency in water >1 MHz, SiN_x membranes with widths below 50 μm are likely required. The strong reduction in frequency is associated with a heavy water loading effect, reaching mass ratios of $m_{\mathrm{wat}}/m_{\mathrm{mem}} \sim 10^2$. The NAVMI factor reaches values close to $\Gamma \sim 1$ for the first (1,1) mode, indicating that the water layer l_w following the membrane motion is close in magnitude to the membrane width, i.e. $l_w \sim$a. Lower NAVMI values in the 0.2-0.4 range are obtained for higher modes. Based on the estimated Reynolds number, $R_e >$3000, for the membranes studied, we infer that the main losses are due to acoustic radiation with limited effect from water viscosity. This is supported by the large NAVMI value for the (1,1) mode. This is a positive aspect for membranes as acoustic metamaterials components, suggesting a good coupling between membrane motion and acoustic waves. The damping coefficients for the (1,1) mode for 40 μm membranes is $\sim 10^{-4}$, with higher values as the membrane width increases. These may indicate that smaller membranes with higher resonance frequencies above 1 MHz will not be severely affected by damping effects. The presented NAVMI factor and damping coefficients can serve as guidelines to design membranes for negative acoustic metamaterials operating in the MHz range for medical ultrasound applications. Further studies are required to analyse the coupling between the membrane vibration and acoustic radiation. An effective energy transfer from the membrane motion towards acoustic radiation would favor the manipulation of acoustic fields through negative metamaterials based on membranes.

SUPPLEMENTARY INFORMATION

Supplementary Information contains: Fig. SI-1 with SiN_x thickness data from ellipsometry; Fig. SI-2 with a SEM cross section of SiN_x layer and the backside morphology of suspended SiN_x membrane; Fig. SI-3 and SI-4 showing the superposition of modes (3,1) with (1,3), and (2,1) with (1,2), respectivly; Fig. SI-5 with plots with resonance frequency for different membrane widths and vibration modes from experimental measurements and simulations; Table SI-1 that contains results from different membrane widths and modes with analytical values of resonance frequency in air, experimental values of resonance frequency in air, experimental values of resonance frequency in water, Q factor in air, and Q factor in water; Fig. SI-6 showing $f_{1,1}^{\mathrm{air}}$ and $f_{1,1}^{\mathrm{water}}$ and the ratio of the frequencies ($f_{1,1}^{\mathrm{air}}/f_{1,1}^{\mathrm{water}}$) in air and water for simulated circular membranes;

ACKNOWLEDGMENTS

This work was supported by the Center for Brain Activity Mapping of the University of California San Diego, and by DARPA under the agreement D18AP00062. It was also generously supported by a research grant from the W.M. Keck Foundation. This work was performed in part at the San Diego Nanotechnology Infrastructure (SDNI) of UCSD, a member of the National Nanotechnology Coordinated Infrastructure, supported by the National Science Foundation (Grant ECCS–1542148).

REFERENCES

[1] Steven A. Cummer, Johan Christensen, and Andrea Alù. Controlling sound with acoustic metamaterials. *Nature Reviews Materials*, 1(3):16001, 2016.

[2] G. Ma and P. Sheng. Acoustic metamaterials: From local resonances to broad horizons. *Science Advances*, 2(2):e1501595–e1501595, 2016.

[3] Sam H Lee and Oliver B Wright. Origin of negative density and modulus in acoustic metamaterials. *Physical Review B*, 93(2):024302, 2016.

[4] Sam Hyeon Lee, Choon Mahn Park, Yong Mun Seo, Zhi Guo Wang, and Chul Koo Kim. Acoustic metamaterial with negative density. *Physics Letters, Section A: General, Atomic and Solid State Physics*, 2009.

[5] Chen Shen, Yangbo Xie, Ni Sui, Wenqi Wang, Steven A Cummer, and Yun Jing. Broadband acoustic hyperbolic metamaterial. *Physical review letters*, 115(25):254301, 2015.

[6] Nicholas Fang, Dongjuan Xi, Jianyi Xu, Muralidhar Ambati, Werayut Srituravanich, Cheng Sun, and Xiang Zhang. Ultrasonic metamaterials with negative modulus. *Nature Materials*, 5(6):452–456, 2006.

[7] Frédéric Bongard, Hervé Lissek, and Juan R Mosig. Acoustic transmission line metamaterial with negative/zero/positive refractive index. *physical Review B*, 82(9):094306, 2010.

[8] Sam Hyeon Lee, Choon Mahn Park, Yong Mun Seo, Zhi Guo Wang, and Chul Koo Kim. Composite acoustic medium with simultaneously negative density and modulus. *Physical review letters*, 104(5):054301, 2010.

[9] Chen Shen, Jun Xu, Nicholas X Fang, and Yun Jing. Anisotropic complementary acoustic metamaterial for canceling out aberrating layers. *Physical Review X*, 4(4):041033, 2014.

[10] E Cianci, A Schina, A Minotti, S Quaresima, and V Foglietti. Dual frequency pecvd silicon nitride for fabrication of cmuts' membranes. *Sensors and Actuators A: Physical*, 127(1):80–87, 2006.

[11] Annette Lohfink and P-C Eccardt. Linear and nonlinear equivalent circuit modeling of cmuts. *IEEE transactions on ultrasonics, ferroelectrics, and frequency control*, 52(12):2163–2172, 2005.

[12] Byung Lee, Amin Nikoozadeh, Kwan Park, and Butrus Khuri-Yakub. High-efficiency output pressure performance using capacitive micromachined ultrasonic transducers with substrate-embedded springs. *Sensors*, 18(8):2520, 2018.

[13] Hao Nan, Kevin C Boyle, Nikhil Apte, Miaad S Aliroteh, Anshuman Bhuyan, Amin Nikoozadeh, Butrus T Khuri-Yakub, and Amin Arbabian. Non-contact thermoacoustic detection of em-

bedded targets using airborne-capacitive micromachined ultrasonic transducers. *Applied Physics Letters*, 106(8):084101, 2015.

[14]O. Vazquez-Mena, L. Gross, S. Xie, L.G. Villanueva, and J. Brugger. Resistless nanofabrication by stencil lithography: A review. *Microelectronic Engineering*, 132:236 – 254, 2015. Micro and Nanofabrication Breakthroughs for Electronics, MEMS and Life Sciences.

[15]Tolga Bagci, Anders Simonsen, Silvan Schmid, Luis G Villanueva, Emil Zeuthen, Jürgen Appel, Jacob M Taylor, A Sørensen, Koji Usami, Albert Schliesser, et al. Optical detection of radio waves through a nanomechanical transducer. *Nature*, 507(7490):81, 2014.

[16]Hien D Tong, Henri V Jansen, Vishwas J Gadgil, Cazimir G Bostan, Erwin Berenschot, Cees JM van Rijn, and Miko Elwenspoek. Silicon nitride nanosieve membrane. *Nano letters*, 4(2):283–287, 2004.

[17]Oscar Vazquez-Mena, Guillermo Villanueva, Veronica Savu, Katrin Sidler, MAF Van Den Boogaart, and Juergen Brugger. Metallic nanowires by full wafer stencil lithography. *Nano Letters*, 8(11):3675–3682, 2008.

[18]P.J French, P.M Sarro, R Mallée, E.J.M Fakkeldij, and R.F Wolffenbuttel. Optimization of a low-stress silicon nitride process for surface-micromachining applications. *Sensors and Actuators A: Physical*, 58(2):149 – 157, 1997.

[19]O. Oralkan, S. T. Hansen, B. Bayram, G. G. Yaralioglu, A. S. Ergun, and B. T. Khuri-Yakub. High-frequency cmut arrays for high-resolution medical imaging. In *IEEE Ultrasonics Symposium, 2004.*, volume 1, pages 399–402 Vol.1, 2004.

[20]Kevin Brenner, Arif Sanli Ergun, Kamyar Firouzi, Morten Fischer Rasmussen, Quintin Stedman, and Butrus (Pierre) Khuri–Yakub. Advances in capacitive micromachined ultrasonic transducers. *Micromachines*, 10(2), 2019.

[21]Bernd Folkmer, Peter Steiner, and Walter Lang. A pressure sensor based on a nitride membrane using single-crystalline piezoresistors. *Sensors and Actuators A: Physical*, 54(1-3):488–492, jun 1996.

[22]M. Amabili and M.K. Kwak. Free vibrations of circular plates coupled with liquids: Revising the lamb problem. *Journal of Fluids and Structures*, 10(7):743 – 761, 1996.

[23]Moon K Kwak. Hydroelastic vibration of rectangular plates. *Journal of applied mechanics*, 63(1):110–115, 1996.

[24]L. G. Villanueva and S. Schmid. Evidence of surface loss as ubiquitous limiting damping mechanism in sin micro- and nanomechanical resonators. *Phys. Rev. Lett.*, 113:227201, Nov 2014.

[25]John Elie Sader. Frequency response of cantilever beams immersed in viscous fluids with applications to the atomic force microscope. *Journal of Applied Physics*, 84(1):64–76, 1998.

[26]Ali H Nayfeh and Mohammad I Younis. A new approach to the modeling and simulation of flexible microstructures under the effect of squeeze-film damping. *Journal of Micromechanics and Microengineering*, 14(2):170, 2003.

[27]Chuanli Zhang, Guanshui Xu, and Qing Jiang. Characterization of the squeeze film damping effect on the quality factor of a microbeam resonator. *Journal of Micromechanics and Microengineering*, 14(10):1302, 2004.

[28]John E Sader, Julian A Sanelli, Brian D Adamson, Jason P Monty, Xingzhan Wei, Simon A Crawford, James R Friend, Ivan Marusic, Paul Mulvaney, and Evan J Bieske. Spring constant calibration of atomic force microscope cantilevers of arbitrary shape. *Review of Scientific Instruments*, 83(10):103705, 2012.

[29]A De Pastina, D Maillard, and LG Villanueva. Fabrication of suspended microchannel resonators with integrated piezoelectric transduction. *Microelectronic Engineering*, 192:83–87, 2018.

[30]William Connacher, Naiqing Zhang, An Huang, Jiyang Mei, Shuai Zhang, Tilvawala Gopesh, and James Friend. Micro/nano acoustofluidics: materials, phenomena, design, devices, and applications. *Lab on a Chip*, 2018.

[31]MR Haddara and S Cao. A study of the dynamic response of submerged rectangular flat plates. *Marine Structures*, 9(10):913–933, 1996.

[32]Liang Sun, Ning Wang, Chong Meng, and Z Yang. High ultrasonic transmission loss metasurfaces in water. *arXiv preprint arXiv:1701.07923*, 2017.

[33]MJ Holmes, NG Parker, and MJW Povey. Temperature dependence of bulk viscosity in water using acoustic spectroscopy. In *Journal of Physics: Conference Series*, volume 269, page 012011. IOP Publishing, 2011.

[34]Robert D Blevins. *Formulas for dynamics, acoustics and vibration*. John Wiley & Sons, 2015.

[35]Abdelhamid Maali, Cedric Hurth, Rodolphe Boisgard, Cédric Jai, Touria Cohen-Bouhacina, and Jean-Pierre Aimé. Hydrodynamics of oscillating atomic force microscopy cantilevers in viscous fluids. *Journal of Applied Physics*, 97(7):074907, apr 2005.

[36]Zhangming Wu and Xianghong Ma. Dynamic analysis of submerged microscale plates: the effects of acoustic radiation and viscous dissipation. *Proceedings of the Royal Society A: Mathematical, Physical and Engineering Sciences*, 472(2187):20150728, 2016.

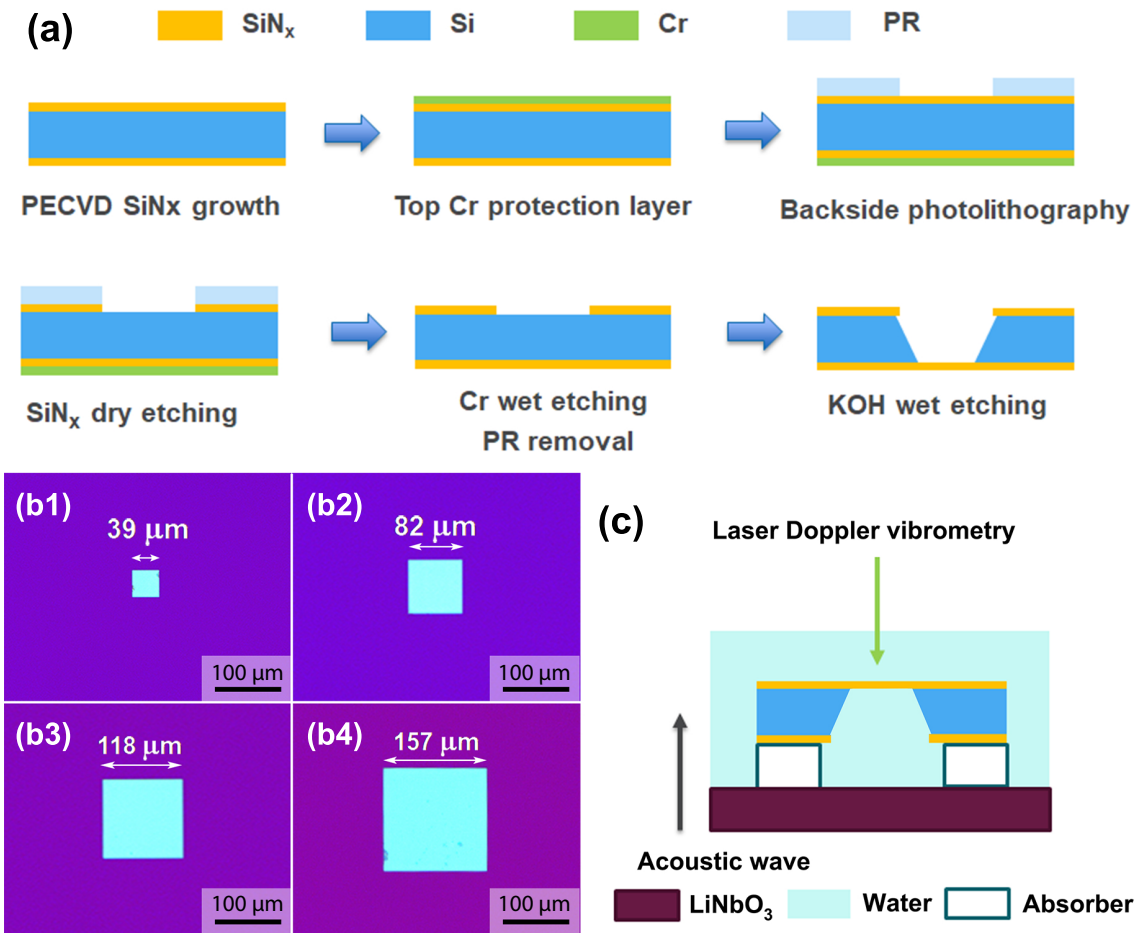

FIG. 1. (a) Process flow for the microfabrication of suspended silicon nitride membranes using photolithography to define etching windows, followed by KOH wet etching of Si for membrane release. (b1)-(b4) Optical image of SiN_x membranes with different membrane widths of 39 µm, 82 µm, 118 µm and 157 µm; Scale bar: 100 µm, (c) LDV experiment setup for resonance frequency measurements.

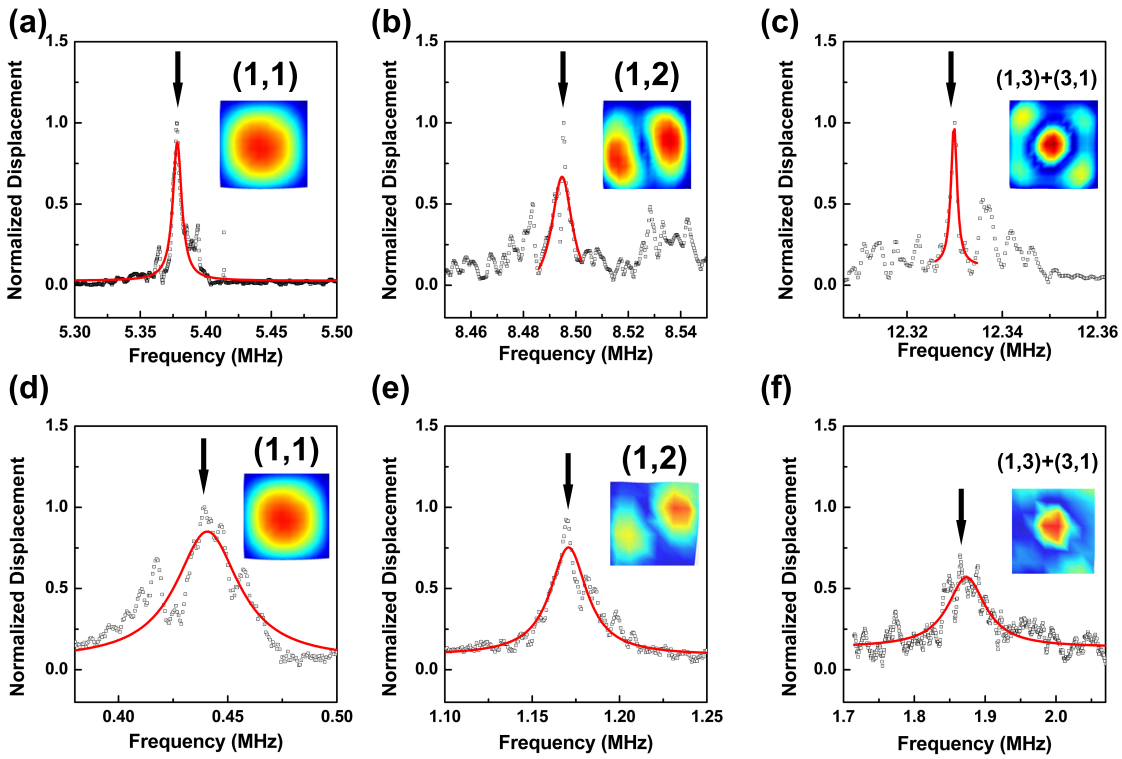

FIG. 2. SiN_x membrane characterization: (a)-(c) Measured resonance frequency and mode shapes by LDV of an 82 μm-square SiN_x membrane in air. (d)-(f) Measured resonance frequency and mode shapes by LDV of the same membrane in water. Red solid lines correspond to Lorentzian fittings.

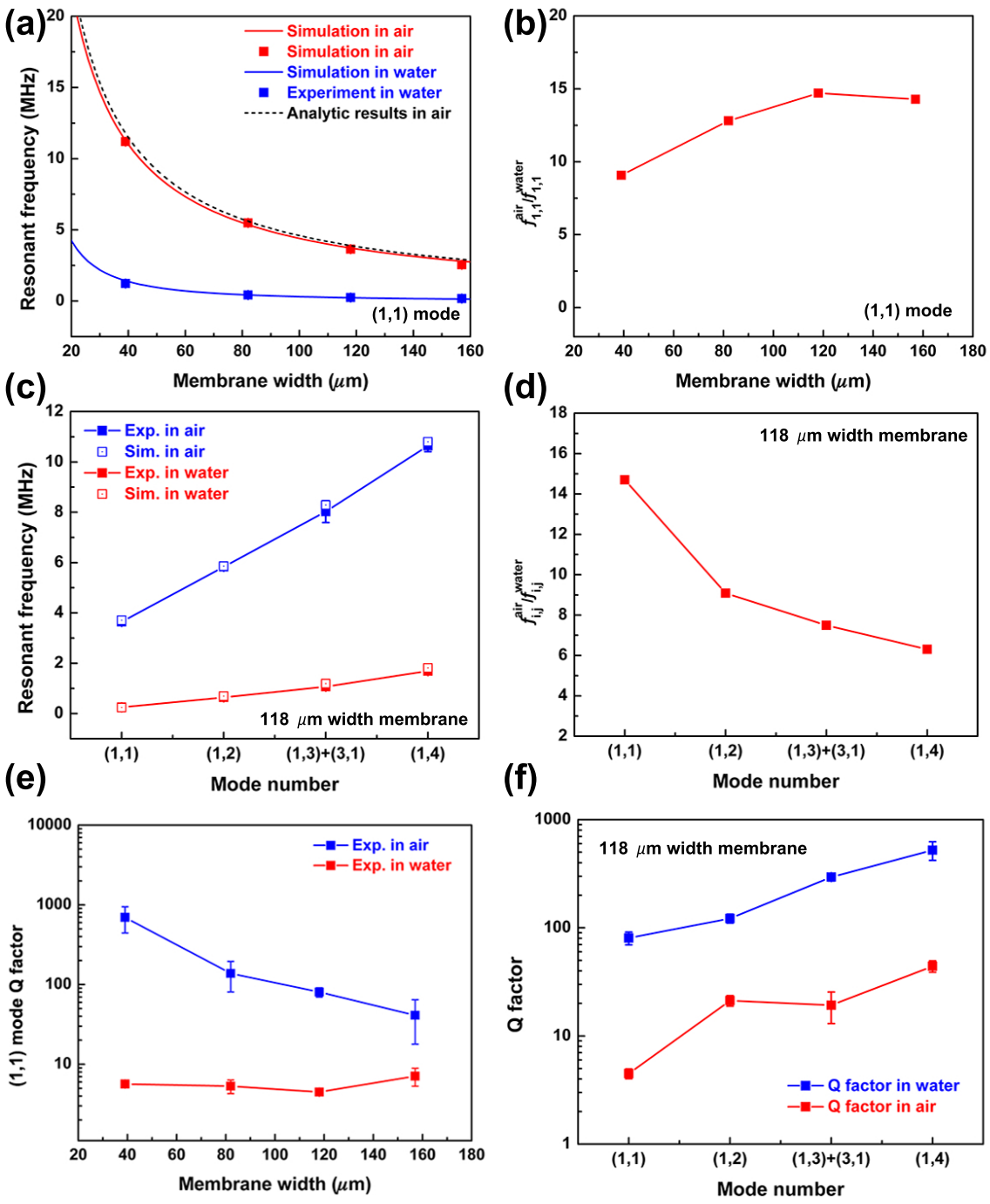

FIG. 3. (a) Resonance frequency as function of membrane width in air and water from LDV measurement, FEM simulations and analytical calculations. (b) Ratio of resonance frequency in air to water $f_{1,1}^{\text{air}}/f_{1,1}^{\text{water}}$ as function of membrane width for (1,1) mode. (c) Resonance frequency for different vibration modes for a membrane 118 μm wide in air and in water. (d) Ratio of resonance frequency in air to water $f_{i,j}^{\text{air}}/f_{i,j}^{\text{water}}$ for different membrane modes of a 118 μm wide membrane. (e) Q factor in air and in water as function of membrane width in air and water for (1,1) mode. (f) Q factor for different vibration modes for a membrane 118 μm wide in air and water.

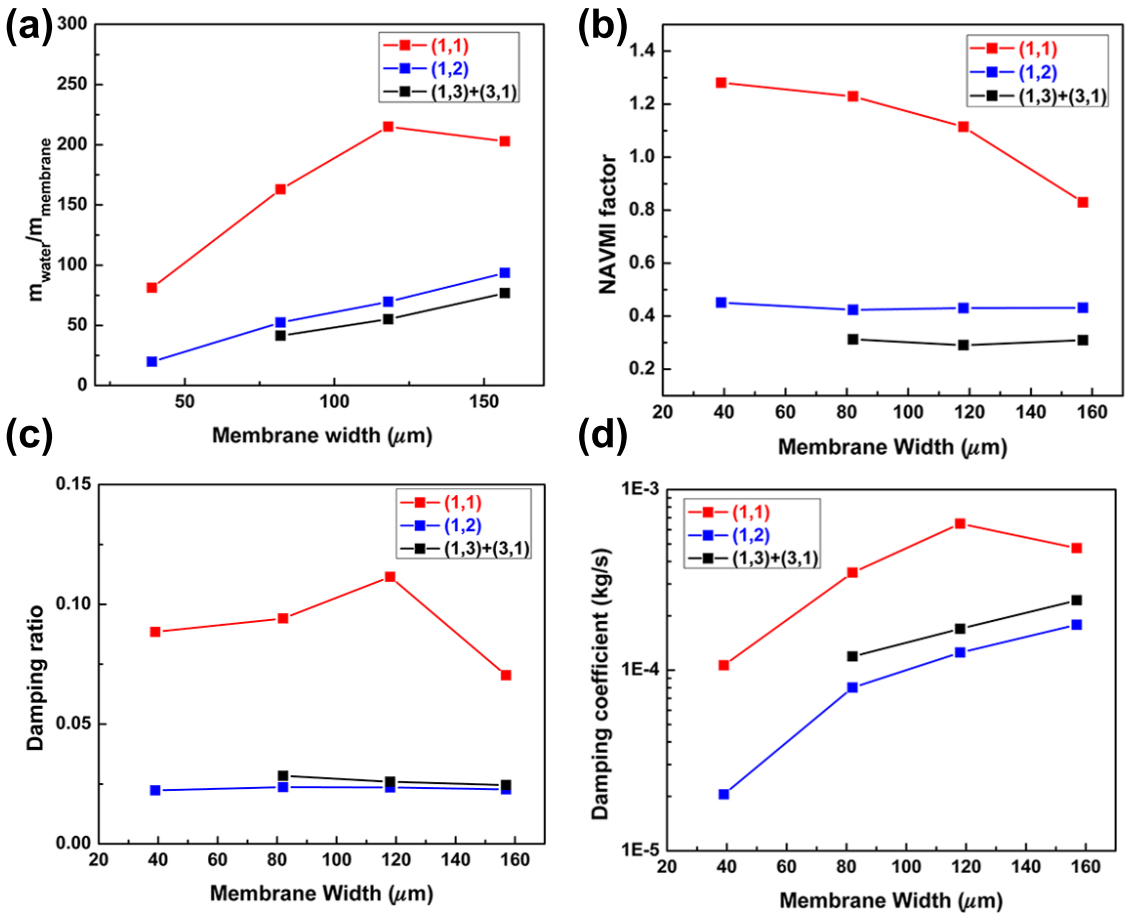

FIG. 4. a) Ratio of added water mass to membrane mass $m_{\mathrm{wat}}/m_{\mathrm{air}}$ as function of membrane width for various vibration modes; b) NAVMI factor as function of width for different vibration modes; c) Damping ratio as function of membrane width for different vibration modes; d) Damping coefficient as function of membrane width for different vibration modes.